Progress In Electromagnetics Research M, Vol. 104, 71–80, 2021

A Rapid Microwave Imaging Approach for the Diagnosis of Traumatic Brain Injury

Bin Li, Heng Liu*, Zekun Zhang, and Xiang Gao

Abstract—This paper presents a method for rapid microwave imaging of traumatic brain injury based on scattering parameters. The algorithm uses the integer order Bessel function and Born approximation, which converts nonlinear inverse scattering problem into linear problem. After truncated singular value decomposition, imaging can be performed without iteration. Simulations and experiments show that the algorithm can not only reduce the amount of calculation for fast imaging, but also accurately image a brain hematoma or foreign body.

1. INTRODUCTION

Traumatic brain injury is one of the most common clinical traumas, with the characteristics of high incidence, high mortality, and high disability rate [1]. If the craniocerebral injury is treated in time, the pressure on the brain can be relieved as soon as possible, and the formation of secondary cerebral ischemia and cerebral herniation can be effectively prevented. Therefore, for brain injuries, timely and efficient detection and treatment are essential [2, 3].

At present, the mainstream diagnostic methods for traumatic brain injury mainly include computed tomography (CT) and nuclear magnetic resonance imaging (MRI), but both of them have the disadvantages of bulkiness and poor portability. There is ionizing radiation in CT detection, which may cause a little harm to the person. The spatial resolution of MRI is not as high as that of CT, and it is relatively expensive and requires a longer scan time. This makes these two technologies fail to meet people's needs for safe, convenient, real-time and high-efficiency diagnostic methods for traumatic brain injury.

Nowadays, biomedical microwave imaging technology gets more and more attention from researchers. Compared with CT and MRI, microwave imaging has the advantages of safe use, no radiation damage, low equipment cost, and easy portability. The research of microwave confocal imaging technology has progressed earlier and faster in brain imaging. Researchers at the University of Queensland proposed a method of using the Finite Difference Time Domain (FDTD) method to simulate and calculate the scattering field parameters excited by the human brain, and then using the microwave confocal imaging algorithm to reconstruct the two-dimensional image of the brain [4, 5]. Since then, researchers have successively tried to image strokes based on microwave confocal imaging algorithms [6, 7]. The key technology of confocal imaging algorithm has also made certain breakthroughs, especially in the elimination of clutter, surface estimation, virtual array technology, and other methods, which effectively improved the accuracy of imaging [8–11].

In recent years, inverse scattering microwave imaging algorithms have received more and more attention for brain microwave diagnosis. However, the electromagnetic inverse scattering problem is a nonlinear ill-posed inverse problem. The existing Newton and Contrast Source Inversion algorithms require iterative calculations, which take a long time [12–14]. In order to diagnose traumatic brain

Received 11 June 2021, Accepted 9 August 2021, Scheduled 18 August 2021
* Corresponding author: Heng Liu (lhengzzt@bit.edu.cn).
The authors are with the School of Information and Electronics, Beijing Institute of Technology, Beijing, China.

injury in time, the imaging method based on Born approximation is proposed, but the brain model used is generally very simple [15].

This paper proposes an algorithm for rapid microwave imaging of craniocerebral injury. Based on the Born approximation, the algorithm avoids nonlinear inverse scattering problem, which reduces computational complexity. Furthermore, it can efficiently map the energy distribution in the three-layer brain model and accurately identify the location of foreign bodies or blood clots.

This paper is organized as follows. Section 2 briefly introduces the choice of working frequency band and three-layer brain model. Section 3 explains the fast microwave imaging algorithm in detail, which uses the Born approximation to linearize the nonlinear inverse scattering problem. Section 4 describes the specific simulation implementation and experimental verification. Finally, Section 5 gives a summary.

2. ULTRA-WIDEBAND ANTENNA AND BRAIN MODEL

2.1. Ultra-Wideband Antenna for Imaging

As shown in Figure 1(a), the ultra-wideband bow-tie antenna fed by coplanar waveguide is designed for better microwave diagnosis of craniocerebral injury. The antenna uses the bow-tie-shaped opening angle to broaden the equivalent width of the two arms of the antenna, and to achieve the fusion of multiple resonance modes by appropriately extending the antenna length. In addition, the coplanar waveguide transmission line is embedded in the arm of the bow-tie, which not only has a small effect on the surface current distribution of the antenna, but also achieves a better conversion of the feed end from unbalanced to balanced. The antenna substrate is made of FR4 material with a thickness of 1 mm. The values of the different dimensions of the antenna mentioned in the geometric structure are as follows (in mm): $L = 56.5$, $W = 57$, $H = 1$, $w_1 = 1$, $g_1 = 1.5$, $w_2 = 7.5$, and $g_2 = 1$.

Figure 1(b) shows the change characteristics of return loss with frequency obtained by three-dimensional full-wave simulation analysis. It can be seen that in the frequency range of 0.52–4 GHz, the return loss is less than -10 dB. The working frequency band of the microwave signal will directly affect the results of brain imaging. The higher the signal frequency is, the shorter the wavelength is, which means a higher resolution [16]. But at the same time the attenuation in propagation will also become larger, that is, the penetration ability of signal becomes weaker. Therefore, these two factors need to be considered comprehensively. For this reason, we measure scattering parameter for imaging at frequency $f = 0.6$ GHz.

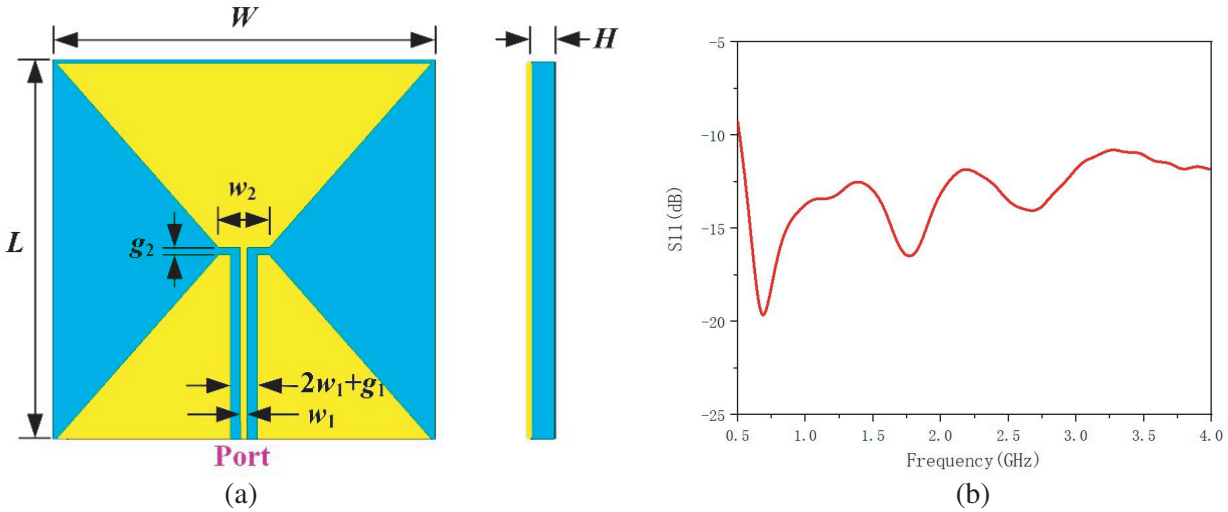

Figure 1. Coplanar waveguide-fed ultra-wideband bow-tie antenna. (a) Geometric structure. (b) Return loss with frequency.

2.2. Brain Model Based on Electromagnetic Properties

The electromagnetic properties of the human brain mainly include relative permittivity ϵ_r and electrical conductivity σ. In order to simplify the modeling complexity of the brain model and verify the feasibility of rapid microwave imaging, we use cross-sectional slices of the brain to simplify the three-dimensional brain problem into a two-dimensional brain model with a radius of 10 cm. At the same time, it assumes that different brain tissues and the blood clot are a homogeneous medium, and its relative permittivity and electrical conductivity are constant [17]. We use a three-layer brain model, which includes skin, skull, and a mixture of brain gray matter and white matter. According to Debye equation, the electromagnetic properties of the three-layer brain model are shown in Table 1.

Table 1. Electromagnetic properties of the three-layer brain model.

Tissue	ϵ_r	σ (S/m)	Range (cm)
Skin	43.6	0.7	9.5–10
Bone	12.8	0.1	9.2–9.5
Mixture of brain gray and white matter	43.2	0.7	0–9.2
Blood clot	58	2.3	/
Matching medium	40	0.9	/

The three-layer brain model and the deployment diagram of the antennas are shown in Figure 2. The yellow area represents the skin; the white area represents the bone; the gray area represents the mixture of brain gray matter and white matter; the small red circle represents a blood clot; the light blue area is the matching medium; and the small black circles represent antennas placed evenly in the matching medium.

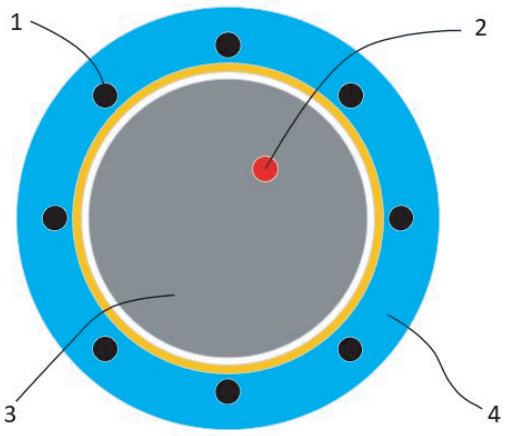

Figure 2. Three-layer brain model and deployment diagram of antennas: 1) antenna, 2) blood clot, 3) three-layer brain model and 4) matching medium.

3. FAST MICROWAVE IMAGING ALGORITHM

In this section, the proposed method for rapid microwave imaging of traumatic brain injury based on scattering parameters is introduced in detail. In order to reduce the amount of calculation, the algorithm uses the Born approximation method to linearize the nonlinear inverse scattering problem.

Firstly, N antennas are placed evenly outside the brain. When one dipole antenna transmits microwave signals, all the antennas receive and calculate the corresponding scattering parameters. The

measured scattering parameters are constructed into the following scattering matrix T, whose size is $N * N$:

$$T = \begin{bmatrix} Sscat(1,1) & Sscat(1,2) & \dots & Sscat(1,N-1) & Sscat(1,N) \\ Sscat(2,1) & Sscat(2,2) & \dots & Sscat(2,N-1) & Sscat(2,N) \\ \vdots & \vdots & \ddots & \vdots & \vdots \\ Sscat(N,1) & Sscat(N,2) & \dots & Sscat(N,N-1) & Sscat(N,N) \end{bmatrix} \tag{1}$$

where $Sscat(m,n)$ represents the scattered-field S parameter when the n-th dipole antenna transmits the microwave signal, and the m-th dipole antenna receives. The elements on the diagonal of the scattering matrix T are simultaneously affected by hematoma and antennas [18]. In order to reduce the influence of the antenna on the imaging, the elements on the diagonal of the scattering matrix T are set to 0, then T is:

$$T = \begin{bmatrix} 0 & Sscat(1,2) & \dots & Sscat(1,N-1) & Sscat(1,N) \\ Sscat(2,1) & 0 & \dots & Sscat(2,N-1) & Sscat(2,N) \\ \vdots & \vdots & \ddots & \vdots & \vdots \\ Sscat(N,1) & Sscat(N,2) & \dots & Sscat(N,N-1) & 0 \end{bmatrix} \tag{2}$$

Perform truncated singular value decomposition on the scattering matrix T to obtain the left singular vector corresponding to the largest singular value:

$$T = USV^* = \sum_{m=1}^{N} \lambda_m U_m V_m^* \approx \lambda_1 U_1 V_1^* \tag{3}$$

where λ_m is the singular value of T, U_m the left singular vector, and V_m the right singular vector. Based on the brain model that has been constructed, $Sscat(m,n)$ can be expressed by the following equation [19, 20]:

$$Sscat(m,n) = \frac{-i\pi k^2 r^2}{4\omega\mu_b} \left(\frac{\epsilon(\mathbf{p}) - \epsilon_b}{\epsilon_b} + i\frac{\sigma(\mathbf{p}) - \sigma_b}{\omega\sigma_b} \right) \mathbf{E_{inc}}(\mathbf{a_n}, \mathbf{p}) \cdot \mathbf{E_{tot}}(\mathbf{p}, \mathbf{a_m}) \tag{4}$$

where the wavenumber $k = \omega^2\mu_b(\epsilon_b + \sigma_b/\omega)$; ω is the angular frequency; μ_b, ϵ_b, and σ_b respectively represent the magnetic permeability, relative permittivity, and electrical conductivity of the brain; r is the radius of the hematoma; $\mathbf{E_{inc}}(\mathbf{a_n}, \mathbf{p})$ represents the incident electric field formed by the dipole antenna a_n at the point p.

Since the radius of the brain hematoma is generally smaller than the wavelength of the detection signal, by applying the Born approximation [21], Equation (4) can be approximated as:

$$Sscat(m,n) \approx \frac{-i\pi k^2 r^2}{4\omega\mu_b} \left(\frac{\epsilon(\mathbf{p}) - \epsilon_b}{\epsilon_b} + i\frac{\sigma(\mathbf{p}) - \sigma_b}{\omega\sigma_b} \right) \mathbf{E_{inc}}(\mathbf{a_n}, \mathbf{p}) \cdot \mathbf{E_{inc}}(\mathbf{p}, \mathbf{a_m}) \tag{5}$$

Furthermore, $\mathbf{E_{inc}}(\mathbf{a_n}, \mathbf{p})$ can be represented by Hankel function:

$$\mathbf{E_{inc}}(\mathbf{a_n}, \mathbf{p}) = \frac{-i}{4} H_0^{(1)}(k|\mathbf{a_n} - \mathbf{p}|) \tag{6}$$

$$\mathbf{F}(\mathbf{p}) = [\mathbf{E_{inc}}(\mathbf{a_1}, \mathbf{p}), \mathbf{E_{inc}}(\mathbf{a_2}, \mathbf{p}), \dots, \mathbf{E_{inc}}(\mathbf{a_n}, \mathbf{p})] \tag{7}$$

where $\mathbf{F}(\mathbf{p})$ represents the incident electric field formed by dipole antennas at different positions; $\mathbf{a_n}$ is the position vector of the n-th dipole antenna; $\mathbf{a_n} = |\mathbf{a_n}|(\cos\theta_n + i\sin\theta_n)$; $|\mathbf{a_n}|$ represents the distance from the n-th dipole antenna to the center of the brain; and θ_n represents the angle between the n-th dipole antenna and the X axis of the Cartesian coordinate system with the center of the brain imaging area as the origin. $\mathbf{p}$ is the vector from the center of the brain imaging area to the imaging point p and represents the position of the imaging point p. $H_0^{(1)}$ is the zero-order Hankel function of the first kind, when $|\mathbf{a_n} - \mathbf{p}| \gg 0.25/k$:

$$H_0^{(1)}(k|\mathbf{a_n} - \mathbf{p}|) \approx \frac{1+i}{4\sqrt{k\pi}} \frac{e^{ik|a_n|}}{\sqrt{|\mathbf{a_n}|}} e^{-ik\theta_n \cdot \mathbf{p}} \tag{8}$$

It can be seen from Equation (5) that when the scattering matrix is subjected to singular value decomposition:

$$U'_m = \overline{V'}_m \approx \mathbf{F}(\mathbf{p}) \tag{9}$$

$\mathbf{F}(\mathbf{p})$ can be expressed by the first kind of zero-order Hankel function, then:

$$U_m = \overline{V}_m \approx \frac{1}{\sqrt{N}} \left[e^{-ik\theta_1 \cdot \mathbf{p}}, e^{-ik\theta_2 \cdot \mathbf{p}}, \ldots, e^{-ik\theta_N \cdot \mathbf{p}} \right] \tag{10}$$

$Sscat(m, n)$ is mainly affected by blood clot in the brain, and suppose that the pixels in the blood clot in the brain are p', so:

$$U_m = \overline{V}_m \approx \frac{1}{\sqrt{N}} \left[e^{-ik\theta_1 \cdot \mathbf{p}'}, e^{-ik\theta_2 \cdot \mathbf{p}'}, \ldots, e^{-ik\theta_N \cdot \mathbf{p}'} \right] \tag{11}$$

In order to determine the location of the traumatic brain injury, the following calculations are performed for each pixel in the brain:

$$Image(p) = \frac{|\langle U_1, G(\mathbf{p}) \rangle|}{\parallel U_1 \parallel \parallel G(\mathbf{p}) \parallel} \tag{12}$$

where $G(\mathbf{p}) = \frac{\mathbf{F}(\mathbf{p})}{|\mathbf{F}(\mathbf{p})|}$, $\parallel U_1 \parallel$ and $\parallel G(\mathbf{p}) \parallel$ represent the 2-norm of the vector U_1 and $G(\mathbf{p})$, respectively.

According to the Jacobi-Angel expansion:

$$e^{ix\cos\theta} = J_0(x) + \sum i_s J_s(x) e^{is\theta} \tag{13}$$

and:

$$\theta_n * \left(\mathbf{p} - \mathbf{p}'\right) = \left|\mathbf{p} - \mathbf{p}'\right| * \cos\left(\theta_n - \theta\right) \tag{14}$$

we can evaluate:

$$\begin{aligned} |\langle U_1, G(\mathbf{p}) \rangle| &= \left| -\frac{i}{4N} \frac{1+i}{4\sqrt{k\pi}} \frac{e^{ik|a_n|}}{\sqrt{|\mathbf{a_n}|}} \left[e^{-ik\theta_1 \cdot \mathbf{p}'}, e^{-ik\theta_2 \cdot \mathbf{p}'}, \ldots, e^{-ik\theta_N \cdot \mathbf{p}'} \right] \left[e^{-ik\theta_1 \cdot \mathbf{p}}, e^{-ik\theta_2 \cdot \mathbf{p}}, \ldots, e^{-ik\theta_N \cdot \mathbf{p}} \right]^T \right| \\ &= \left| -\frac{i}{4N} \frac{1+i}{4\sqrt{k\pi}} \frac{e^{ik|a_n|}}{\sqrt{|\mathbf{a_n}|}} \sum_{n=1}^{N} e^{-ik\theta_n \cdot (\mathbf{p} - \mathbf{p}')} \right| \end{aligned} \tag{15}$$

$$|\langle U_1, G(\mathbf{p}) \rangle| = \left| -\frac{i}{4N} \frac{1+i}{4\sqrt{k\pi}} \frac{e^{ik|a_n|}}{\sqrt{|\mathbf{a_n}|}} \left(N J_0\left(k|\mathbf{p} - \mathbf{p}'|\right) \right) + \sum_{n=1}^{N} \sum_{s \in Z \&\& s \neq 0} i^s J_s\left(k|\mathbf{p} - \mathbf{p}'|\right) e^{is(\theta_n - \theta)} \right| \tag{16}$$

where θ represents the angle between brain hematoma and the X axis of the Cartesian coordinate system with the center of the brain imaging area as the origin. Because of the Bessel function $J_0(0) = 1$ and $J_s(0) = 0$ ($s \in Z$ and $s \neq 0$). According to the Holder inequality: $|\langle U_1, G(\mathbf{p}) \rangle| \leq \parallel U_1 \parallel \parallel G(\mathbf{p}) \parallel$ so only when $\mathbf{p} = \mathbf{p}'$ calculating the pixels in the brain injury, $Image(p)$ tends to 1; when calculating the imaging points of the normal part of the brain, $Image(p)$ tends to 0.

4. SIMULATION IMPLEMENTATION AND EXPERIMENTAL VERIFICATION

In order to verify the fast microwave imaging algorithm and imaging performance, the simulation software CST STUDIO SUITE is used to simulate the incident electric field and S parameters. The scattered-field S parameter is the simulated S parameter when the brain has a blood clot minus the S parameter when the brain is normal. When 16 dipole antennas are placed outside the brain area, the simulation setup diagram is shown in Figure 3.

In Figure 3, the big blue circle represents the matching medium; the three-tiered circle represents the brain; and the red circle represents a blood clot. Figure 4 shows the distribution of the singular values of the constructed scattering matrix T. It can be seen that the first non-zero singular value is much larger than the other singular values. It is precisely because of the presence of blood clots in the brain that the first non-zero singular is large. This not only proves the correctness of Equation (3), but also further proves the rationality of the imaging algorithm.

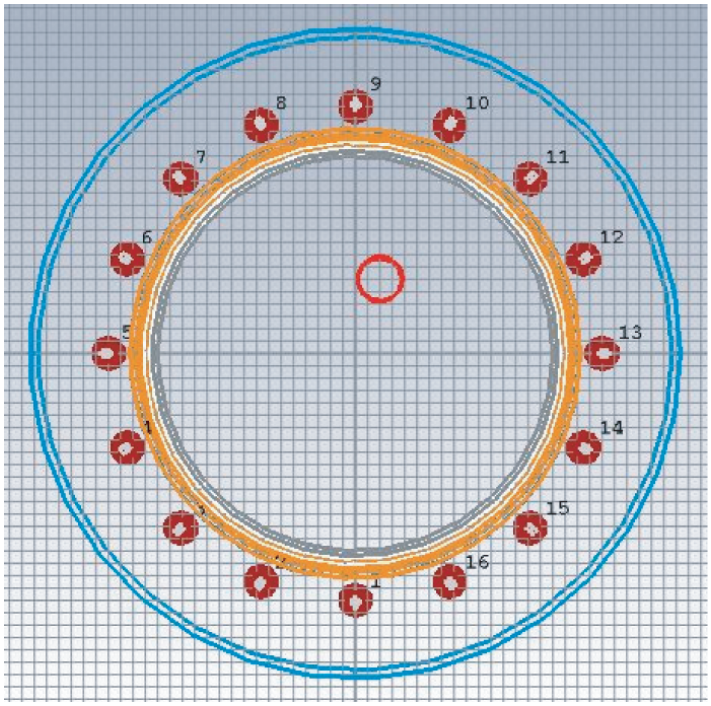

Figure 3. Simulation diagram with 16 antennas.

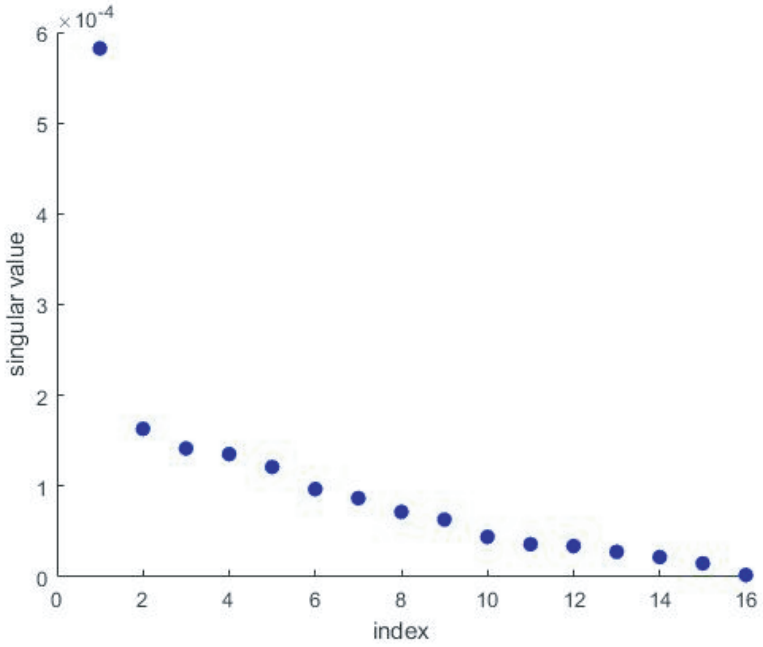

Figure 4. Distribution of singular values.

When the blood clot with a radius of 1 cm is located at the point $(10, 30)$, the imaging result is shown as Figure 5.

The positioning accuracy is used to quantify the performance of the imaging algorithm. The metric $\triangle d$ represents the difference between the center position of the predicted blood clot in the reconstructed

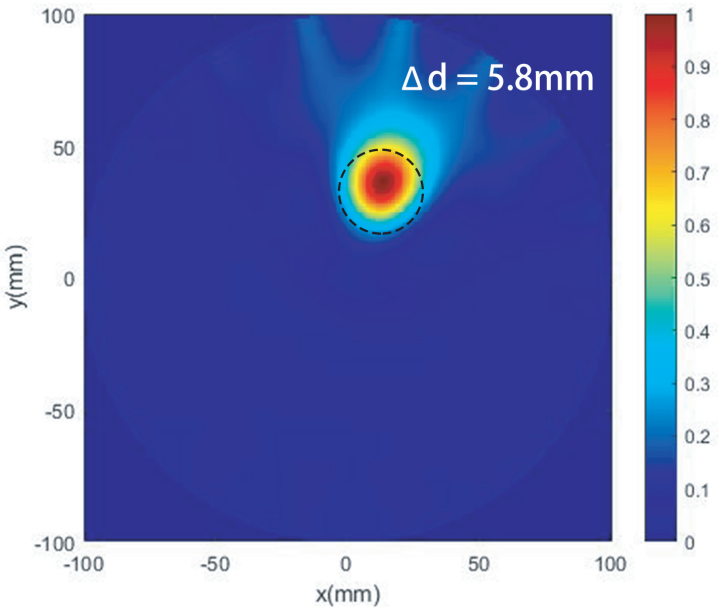

Figure 5. Reconstructed images of simulation.

image and the center position of the blood clot in the model:

$$\triangle d = \| \, TC(x,y) - RC(x,y) \, \| \tag{17}$$

where $TC(x,y)$ represents the center position of the blood clot in the image, and $RC(x,y)$ represents the center position of the blood clot in the model. $\triangle d = 5.8\,\text{mm}$ in Figure 5. It can be seen from the simulation results that the method proposed has high positioning accuracy.

The microwave experiment platform is built to further verify the imaging algorithm. As shown in Figure 6, the experiment platform consists of a VNA, laptop, switch matrix, and simplified tested brain

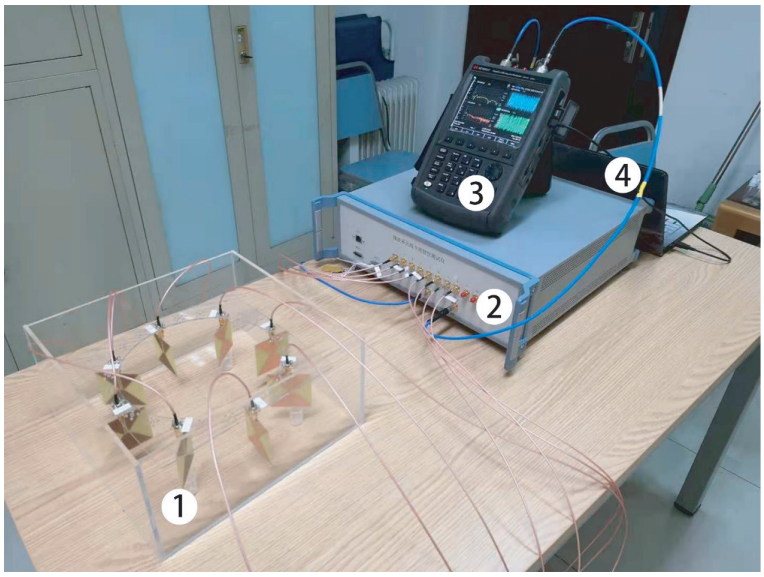

Figure 6. Microwave experiment platform: 1) simplified tested brain model with 8 antennas around, 2) switch matrix, 3) VNA, and 4) laptop.

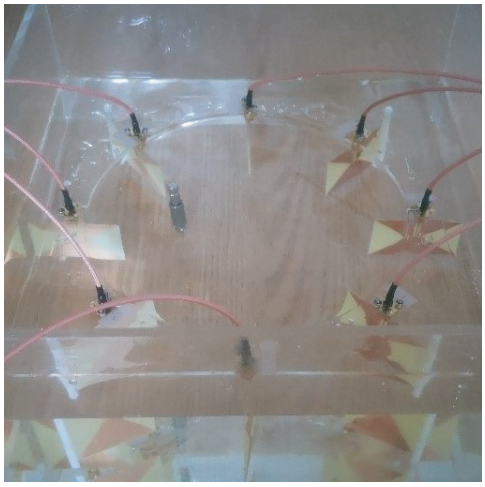

(a)

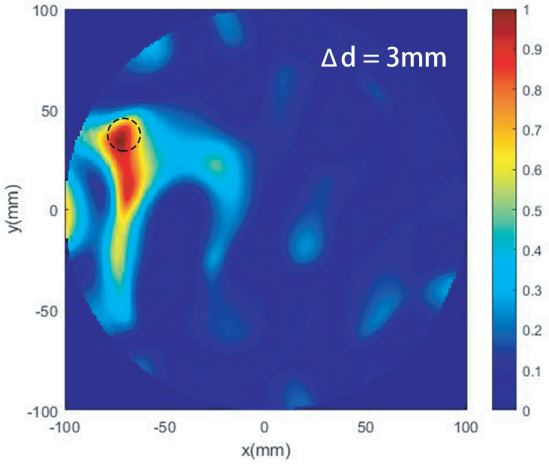

(b)

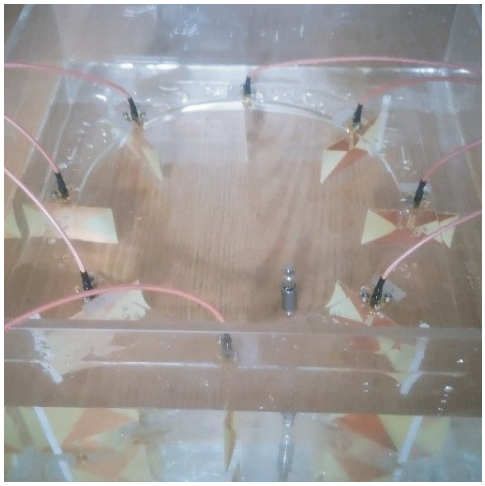

(c)

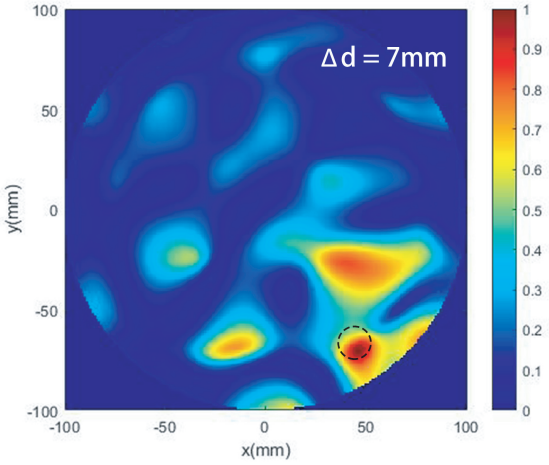

(d)

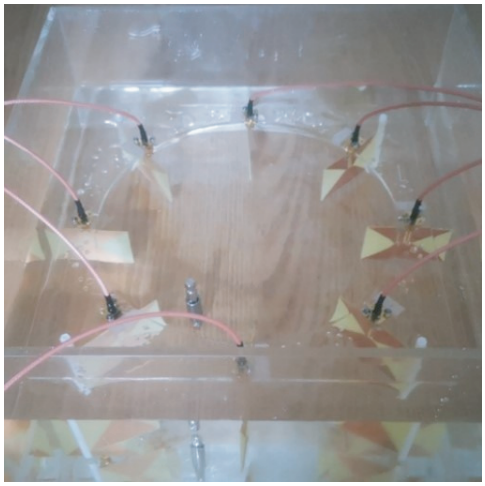

(e)

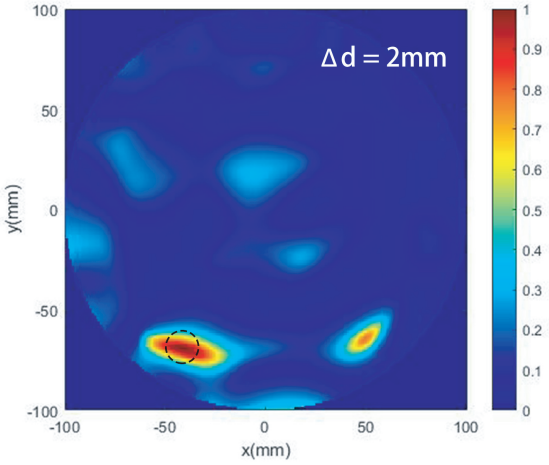

(f)

Figure 7. Validation of the proposed imaging approach. (a), (c), (e) Test chart. (b), (d), (f) Imaging chart.

model with 8 antennas around. The laptop sends commands to the VNA and switch matrix respectively to generate signals and select antennas. In addition, the laptop captures and processes signals from different antennas for imaging.

The simplified tested brain model is a glass container with a radius of 10 cm and a height of 10 cm. Fill it with pure glycerin, and put a metal cylinder with a radius of 5 mm in a specific position in the glycerin to act as a foreign body in the brain. Figure 7 shows the test and imaging results of foreign body in different positions when the frequency $f = 0.55$ GHz.

According to the actual imaging diagram, it can be seen that the proposed microwave imaging method can map the energy distribution in the simplified tested brain model. It accurately detects the existence of a foreign body and predict its location to within a few millimeters.

5. CONCLUSION

A microwave imaging algorithm based on scattering parameters for the detection of craniocerebral injuries in time has been presented. In order to eliminate the influence of the antenna on the imaging effect, the algorithm constructs a scattering matrix without diagonal elements. In addition, it uses Born approximation and the first kind of first-order Hankel function in the frequency domain to calculate power distributions inside the simplified brain model. Thus, the presented approach removes the need to solve time-domain or nonlinear inverse problems. After simulation and experimental verification, the imaging algorithm quickly and accurately locates the location of small blood clots and foreign objects. Future work will include refining the brain model and comparing several competing microwave imaging algorithms.

ACKNOWLEDGMENT

This work was supported by the National Natural Science Foundation of China under Grant No. 61971038.

REFERENCES

1. Hackenberg, K. and A. Unterberg, "Traumatic brain injury," *Der Nervenarzt*, Vol. 87, No. 2, 203–14, 2016.
2. Wintermark, M., P. C. Sanelli, and Y. Anzai, "Imaging evidence and recommendations for traumatic brain injury: Conventional neuroimaging techniques," *Journal of the American College of Radiology*, Vol. 12, No. 2, 1–14, 2015.
3. Heit, J. J., M. Iv, and M. Wintermark, "Imaging of intracranial hemorrhage," *Journal of Stroke*, Vol. 19, No. 1, 11, 2017.
4. Mohammed, B. J., A. M. Abbosh, and D. Ireland, "Circular antenna array for brain imaging systems," *Proceedings of the 2012 IEEE International Symposium on Antennas and Propagation*, 1–2, 2012.
5. Ireland, D. and M. E. Bialkowski, "Microwave head imaging for stroke detection," *Progress In Electromagnetics Research M*, Vol. 21, 163–175, 2011.
6. Zamani, A., A. T. Mobashsher, B. J. Mohammed, and A. M. Abbosh, "Microwave imaging using frequency domain method for brain stroke detection," *IEEE MTT-S International Microwave Workshop Series (IMWS-Bio)*, 1–3, 2014.
7. Mohammed, B. J., A. M. Abbosh, and S. Mustafa, "Microwave system for head imaging," *IEEE Transactions on Instrumentation and Measurement*, Vol. 63, No. 1, 117–123, 2014.
8. Zamani, A., "Fast frequency-based multistatic microwave imaging algorithm with application to brain injury detection," *IEEE Transactions on Microwave Theory and Techniques*, Vol. 64, No. 2, 653–662, 2016.
9. Mobashsher, A. T. and A. Abbosh, "Design of compact cross-fed three-dimensional slotloaded antenna and its application in wideband head imaging system," *IEEE Antennas and Wireless Propagation Letters*, Vol. 15, 1856–1860, 2016.

10. Mohammed, B. J., K. Bialkowski, and S. Mustafa, "Investigation of noise effect on image quality in microwave head imaging systems," *IET Microwaves, Antennas and Propagation*, Vol. 9, No. 3, 200–205, 2015.
11. Zamani, A. and A. M. Abbosh, "Fast multi-static technique for microwave brain imaging," *2015 IEEE International Symposium on Antennas and Propagation and USNC/URSI National Radio Science Meeting*, 536–537, 2015.
12. Fedeli, A., V. Schenone, A. Randazzo, M. Pastorino, T. Henriksson, and S. Semenov, "Nonlinear S-parameters inversion for stroke imaging," *IEEE Transactions on Microwave Theory and Techniques*, Vol. 68, 1760–1771, 2020.
13. Semenov, S. Y. and D. R. Corfield, "Microwave tomography for brain imaging: Feasibility assessment for stroke detection," *International Journal of Antennas and Propagation*, 1–8, 2008.
14. Dilman, İ, U. Yıldırım, S. Coşğun, S. Doğu, M. Çayören, and I. Akduman, "Feasibility of brain stroke imaging with microwaves," *2016 IEEE Asia-Pacific Conference on Applied Electromagnetics (APACE)*, 334–338, 2016.
15. Tobon Vasquez, J. A., R. Scapaticci, G. Turvani, G. Bellizzi, D. O. Rodriguez-Duarte, N. Joachimowicz, B. Duchêne, E. Tedeschi, M. R. Casu, L. Crocco, and F. Vipiana, "A prototype microwave system for 3D brain stroke imaging," *Sensors*, Vol. 20, 2607, 2020.
16. Nikolova, N. K., "microwave imaging for breast cancer," *Microwave Magazine IEEE*, Vol. 12, No. 7, 78–94, 2011.
17. Persson, M., A. Fhager, and H. D. Trefná, "Microwave-based stroke diagnosis making global prehospital thrombolytic treatment possible," *IEEE Transactions on Biomedical Engineering*, Vol. 61, No. 11, 2806–2817, 2014.
18. Park, W. K., "Real-time microwave imaging of unknown anomalies via scattering matrix," *Mechanical Systems and Signal Processing*, Vol. 118, 658–674, 2019.
19. Haynes, M., J. Stang, and M. Moghaddam, "Microwave breast imaging system prototype with integrated numerical characterization," *International Journal of Biomedical Imaging*, Vol. 2012, 1–18, 2012.
20. Haynes, M. and M. Moghaddam, "Vector Green's function for S-parameter measurements of the electromagnetic volume integral equation," *IEEE Trans. Antennas Propagation*, Vol. 60, No. 3, 1400–1413, 2012.
21. Haynes, M., J. Stang, and M. Moghaddam, "Real-time microwave imaging of differential temperature for thermal therapy monitoring," *IEEE Transactions on Biomedical Engineering*, Vol. 61, No. 6, 1787–1797, 2014.